Three-dimensional vorticity modes in the wake of a flat plate

J. C. Lasheras
Department of Mechanical Engineering, University of Southern California, Los Angeles, California 90089-1453

E. Meiburg
Center for Fluid Mechanics, Division of Applied Mathematics, Brown University, Providence, Rhode Island 02912

(Received 31 May 1989; accepted 10 November 1989)

The three-dimensional development of the wake behind a flat plate separating two laminar streams of equal velocity, subjected to perturbations in its initial conditions, is studied experimentally and numerically at moderate Reynolds numbers. The effect of single waves as well as subharmonic streamwise forcing is discussed. For the case of a single wave, streamwise forcing combined with a sinusoidal spanwise perturbation, the two distinct three-dimensional vorticity modes found in an early study [J. Fluid Mech. **190**, 1 (1988)], are further studied and their symmetry properties analyzed. Depending on the orientation of the spanwise perturbation, the counter-rotating pairs of streamwise vortex tubes forming in the braids are shown to induce undulations in the cores of the Karman-like vortices, resulting in either an *in-phase* or a *varicose* configuration. Furthermore, when the wake is subjected to subharmonic streamwise forcing, additional modes of the topology of the vorticity field are shown to exist. The evolution of these subharmonic three-dimensional modes is analyzed as a function of the initial conditions.

I. INTRODUCTION

At moderate and large Reynolds numbers, the wake behind two-dimensional bodies exhibits a coherent vortical structure.[1,2] In addition, it has been found experimentally as well as numerically that after an initial transition period, the wake behind two-dimensional bodies develops a three-dimensional structure. One of the first evidences of this three-dimensional transition was provided by Grant.[3] His correlation measurements indicated that the wake, while exhibiting the two-dimensional Karman-like vortices, also develops a three-dimensional vortical structure composed of counter-rotating pairs of streamwise vortices whose axes are located in planes inclined to the plane of the wake. Similar *vortex-pair* eddy structures have also been described by Payne and Lumley,[4] Townsend,[5] and Mumford,[6] among others. More recently, additional experimental evidence of this three-dimensional structure has been provided by Cimbala *et al.*,[7] Meiburg and Lasheras,[8,9] Detemple,[10] Williamson,[11,12] Ferre and Giralt,[13] Marasli *et al.*,[14] and others.

In order to analyze the three-dimensional transition in the wake behind two-dimensional bodies and, in particular, to study the instability mechanisms leading to this transition, we conducted a combined experimental and numerical investigation of the structure of the near region of the wake developing behind a flat plate subjected to spanwise perturbations.[9] We found that the overall induction of the vorticity emanating from the two sides of the flat plate resulted in the formation of counter-rotating pairs of streamwise vortex tubes that are located in the braids, connecting consecutive Karman vortices of opposite sign. Furthermore, it was noticed that depending on the orientation of the initial spanwise perturbation, the wake acquires two distinct three-dimensional vorticity configurations with different symmetry characteristics. In this paper, we have extended our original work[9] to fully characterize the symmetry properties of the three-dimensional vorticity modes developing in the wake of two-dimensional bodies and their dependence on the initial conditions.

In addition, motivated by recent numerical simulations,[15,16] which demonstrated that vortex pairing may play an important role in the growth of the far-wake structure, we have investigated the effect of the subharmonic streamwise forcing in the three-dimensional evolution of the wake.

For this purpose, we are presenting a comparative study between numerical inviscid vortex dynamics simulations and flow visualizations of the evolution of the wake formed behind a flat plate by two co-flowing laminar streams subjected to spanwise and oblique perturbations of varying amplitude, wavelength, and orientation. Both the effects of single waves and subharmonic streamwise forcing will be discussed.

II. EXPERIMENTAL AND NUMERICAL TECHNIQUES

The flow configuration selected for the study is a plane wake forming behind a flat plate that separates two laminar water streams with equal velocities ($U = 3.4$ cm/sec). At the trailing edge of the splitter plate, the two streams emanating from it have boundary layers 9 mm thick. The Reynolds number based on free-stream velocity and total momentum thickness is 74.

To periodically perturb along the span the two vorticity layers of opposite sign forming the wake, the geometry of the trailing edge of the splitter plate was modified along the span. For the case of a single wave streamwise excitation, three different types of perturbations were investigated. The

 0899-8213/90/030371-10$02.00

first one consisted of gradually corrugating the plate to achieve a small-amplitude, sinusoidal undulation of a given wavelength λ at its trailing edge. This resulted in periodically lifting up and down the two vorticity layers emanating from the plate; thus introducing periodically along the span an in-phase vertical (cross-stream) vorticity-perturbation component in the two layers. The second one consisted of introducing a horizontal (plane of the wake) vorticity-perturbation component in phase in both layers. This was done by serrating the trailing edge of the flat plate to achieve a small-amplitude sinusoidal indentation of a given wavelength λ at its trailing edge. The third type consisted of introducing in the two layers a vorticity perturbation having both horizontal and vertical components. A detailed description of the experimental facility, as well as the geometry of the plates, is given elsewhere.[17–19] For the case of subharmonic streamwise excitation only the cases of a vertical spanwise or oblique vorticity perturbation were studied.

The evolution of the three-dimensional wake was experimentally studied by visualizing the temporal and spatial evolution of the interface that separates the two streams composing the wake. The interface between each stream was visualized by inducing the fluorescence of submicron size particles added to one of the streams either by a laser sheet or by an array of spotlights. A description of this technique is given in Lasheras and Choi.[18]

Comparisons between experimental interface visualizations[18] and numerical calculations[19] have demonstrated that the three-dimensional evolution of low Reynolds number free shear layers developing from laminar streams can be reproduced by numerical inviscid vortex dynamics. Furthermore, we have also shown[9] that this is the case for three-dimensional plane wakes forming between two laminar streams at moderate Reynolds numbers. Thus, to simulate the flow evolution, the two vorticity layers representing the two sides of the wake were discretized into vortex filaments with a circular cross section over which the vorticity is distributed algebraically. The three-dimensional evolution of the two layers of vortex filaments was computed in a Lagrangian frame via the Biot–Savart law. The temporal evolution of the vortex filaments under their global induction was then computed using periodic boundary conditions both in the spanwise and streamwise directions. To allow comparison with the experiments, the three-dimensional position of the interface was also calculated at each time step by keeping track of marker particles initially located at the midplane. The numerical techniques used in the present study are identical in most respects to the ones used by Ashurst and Meiburg.[19] The specific details of the numerical technique can be found in Meiburg and Lasheras.[9]

III. SINGLE WAVE STREAMWISE FORCING: COMPARISON BETWEEN THE TWO VORTICITY MODES OF THE THREE-DIMENSIONAL WAKE

In our previous investigation,[9] we have shown that under the combined effect of both two- and three-dimensional perturbations, the overall induction of the vorticity (concentration, reorientation, and stretching) results in the formation of counter-rotating pairs of streamwise vortices that are located in the braids connecting consecutive Karman vortices of opposite sign (planes inclined to the plane of the wake).

Depending on the orientation of the initial spanwise perturbation, the wake was observed to develop two distinct, three-dimensional vorticity modes of different symmetry properties. Under the global induction of the vorticity, the perturbation vorticity in both layers is reoriented along the directions of positive strain in the evolving strain fields created by the two-dimensional spanwise vortices. When subjected to a vertical (cross-stream) initial spanwise perturbation this induction results in a 180° phase shift between the perturbation vorticity of both layers, leading to a loss of the vertical (x-y plane) symmetry during the initial development of the wake. On the other hand, under the effect of a horizontal (plane of the wake) initial spanwise perturbation, the stretched perturbation vorticity reoriented along the directions of positive strain in both layers is found to remain in phase, preserving the vertical (x-y plane) symmetry of the wake.

The results of the numerical simulation at a time step, $t = 169$, for both the case of the vertical (cross-stream) and horizontal (plane of the wake) sinusoidal perturbations are given in Figs. 1 and 2, respectively. The diameter of the filaments at the start of the simulation represents a measure for

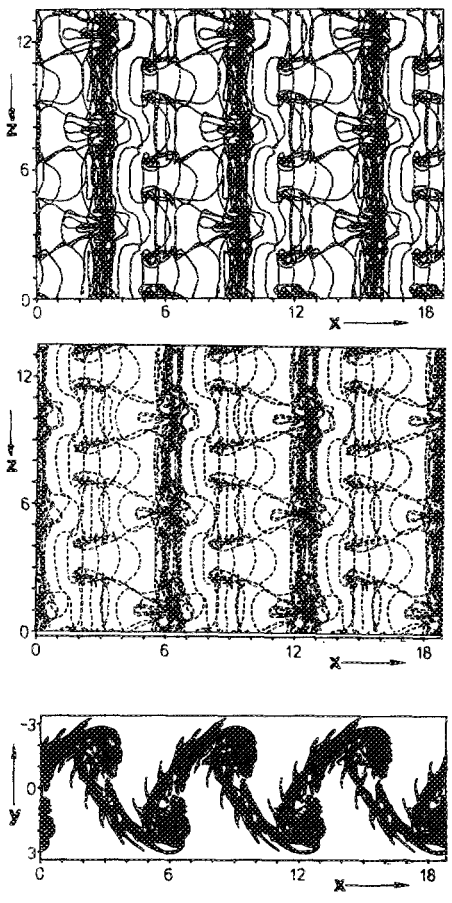

FIG. 1. Sinusoidal, vertically (cross-stream) oriented perturbation. Plan view of the filaments of the upper and lower layers at a time $t = 169$. The side view shows all the filaments of both upper and lower layers.

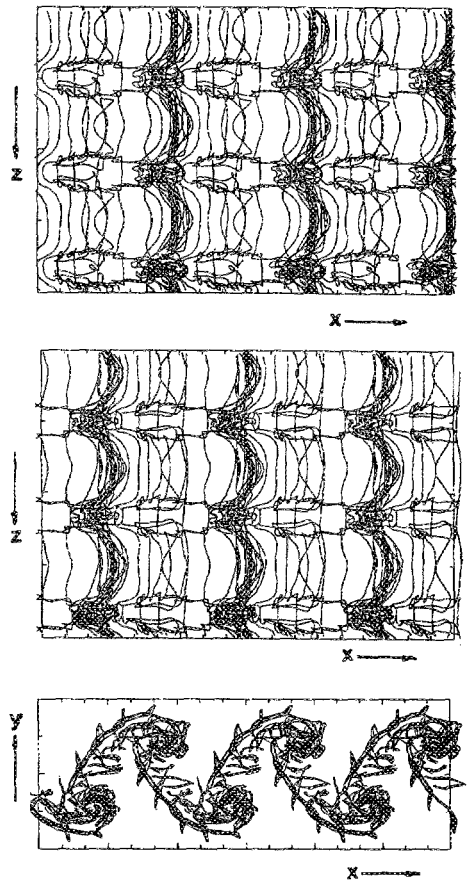

FIG. 2. Sinusoidal, horizontally (plane of the wake) oriented perturbation. Plan view of the filaments of the upper and lower layers at a time $t = 169$. The side view shows all the filaments of both upper and lower layers.

the thickness of the rotational layer and is taken to be the unit length. The two vorticity layers are initially centered at $y = +/-0.65$. The free-stream velocity is taken as the reference velocity, from which the definition of the unit time then follows as the unit length divided by the unit velocity. The case selected for the study corresponds to a wavelength of the spanwise perturbation equal to two-thirds of the two-dimensional streamwise perturbation. At this time, in both cases, the formation of the Karman vortex street has been completed and the appearance in the braids of the streamwise vorticity concentration is clearly seen. For the purpose of clarity, the vortex filaments evolving from the upper and lower layer are given in two separate plan views. Notice that while the side view of the vortex filaments in the two cases reveals a practically identical shape, the plan view of the three-dimensional vortex filaments already shows some important differences. In mode 1 (resulting from the cross-stream perturbation, Fig. 1), the counter-rotating pair of streamwise vortices formed in both layers acquires a *lambda-shaped* form, while in mode 2 (resulting from the perturbation oriented in the plane of the wake, Fig. 2) the counter-rotating pairs of streamwise vortices of both layers remain in the plan view always parallel to the x direction, while their relative distance is not constant across the span.

In a reference frame moving with the average velocity of the evolving Karman-like vortices, the topology of the velocity field shows the presence of free stagnation points in each layer (Figs. 3 and 4). The amplification of the vorticity perturbation, and thus the strength of the generated streamwise vortex pairs, is maximum at the location of the free stagnation points. Because of the staggered organization of the Karman vortices, the free stagnation points of the upper and lower layers are also staggered. Consequently, at one fixed downstream location x, the streamwise vortices generated in the upper and lower layers are not of the same strength. In Fig. 3, the case corresponding to mode 1 is shown, where the stretched perturbation vorticity of both layers is 180° out of phase. At section A–A of the figure, the vortex pairs formed in the upper and lower layer are of equal sign; however, the strength of the streamwise vortices generated from the upper layer is much stronger than from the lower layer. The opposite is the case for section B–B, where the strength of the counter-rotating pairs of vortices generated from the lower layer is greater than that of the upper layer. This unequal strength in the vortex dipoles induces a lateral displacement of the weaker vortices by the stronger ones, as shown in the figure. The result is that at section A–A the distance between the vortex pair 2–3 of the lower layer L_2 is greater than L, while at section B–B, the distance between the pair in the upper layer is smaller than the corresponding one in the lower layer. This induced lateral displacement, which alternates with the strength of the streamwise vortices in the upper and lower layers as we move in the x direction, results in the

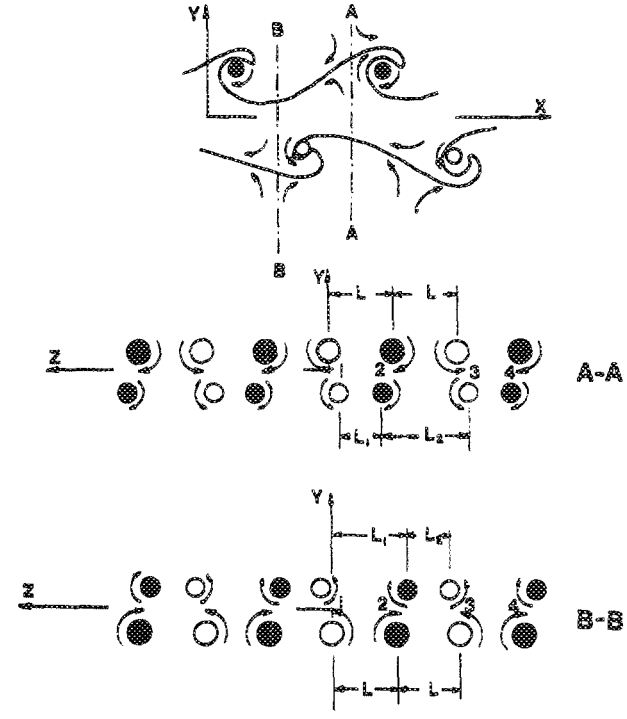

FIG. 3. Mode 1 (sinusoidal, cross-stream perturbation). Observe the unequal spacing between consecutive streamwise vortices that changes as one moves along the streamwise (x) direction (from section B–B to section A–A) producing a A shape in the plan view.

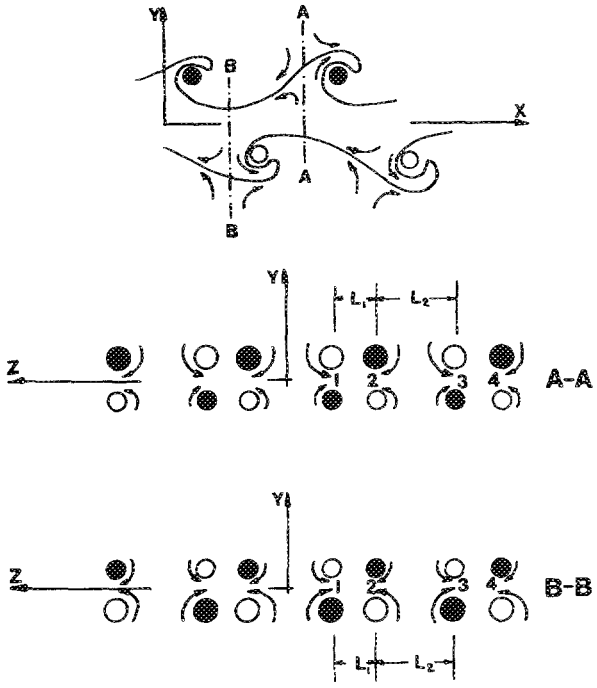

FIG. 4. Mode 2 (sinusoidal, perturbation in the plane of the wake). Notice that the induction of the counter-rotating pairs of streamwise vortices generated in each layer leads to lateral displacements that result in their unequal spacing along the span. This spacing remains constant as one moves along the streamwise direction (from section B–B to section A–A) producing a parallel shape in the plan view.

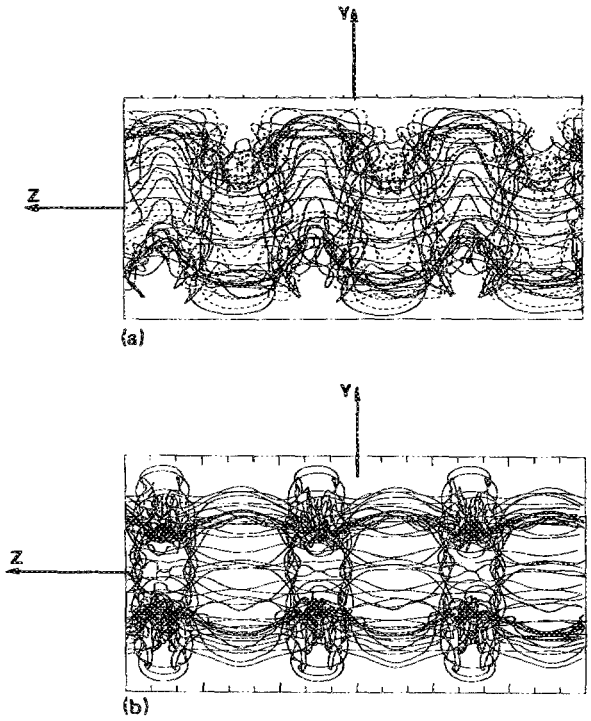

FIG. 5. End view of the filament of the upper and lower layer composing the wake. (a) Mode 1 (sinusoidal, cross-stream perturbation). (b) Mode 2 (sinusoidal perturbation in the plane of the wake). Notice the *in phase* and *varicose* shape of the spanwise, Karman-like vortices in modes 1 and 2, respectively.

observed *lambda*-shaped structure of the streamwise vortex tubes formed in each layer, as shown in Fig. 1. In mode 2, however, the fact that the stretched vorticity perturbation remains in phase in the two layers leads to the vorticity configuration in sections A–A and B–B as given in Fig. 4. Observe now that as was the case with mode 1, the strength of the streamwise vortices of the lower layer in sections A–A is weaker than in the upper layer, while in section B–B the opposite is true (the strength of the streamwise vortices of the lower layer is greater than in the upper layer). However, note that the opposite sign pair of vortices formed at each vertical position induces a lateral displacement of the pairs 1 and 2 closer to each other while pairs 2 and 3 move away from each other. In section B–B, the global induction results in precisely the same lateral displacement, thus maintaining the streamwise vortex tubes parallel to each other, as was shown in Fig. 2. In addition, this lateral displacement lead to an unequal separation along the span between the streamwise vortex pairs ($L_1 \neq L_2$).

In addition, the interaction of the evolving streamwise vortices with the spanwise ones leads to a vertical (x-y plane) undulation in the axis of the spanwise vortices. Figure 5 shows the end view of all the filaments composing the upper and lower layers. Observe that the axes of the Karman vortices are undulated in the vertical plane. In mode 1, this undulation is *in phase* between the Karman vortices of opposite sign, while in mode 2 it is 180° phase shifted, resulting in a *varicose* shape.

These undulations of the axes of the Karman-like vortices described above are clearly seen in both modes 1 and 2 in the lateral perspective views of the visualized interface given in Fig. 6. It should be pointed out that as was shown in our previous work[9] and observed in these interface visualizations, mode 1 evolves from a vertically (x-y plane) antisymmetric configuration whereby the interaction of the streamwise and spanwise vortices leads to a modulation along the span in the strength of the Karman vortices. This modulation in the strength produced during the initial evolution of the three-dimensional instability is 180° phase shifted between the Karman vortices of the opposite sign. However, as will be shown later, as the stretching progresses, the interaction of the streamwise vortices with the spanwise vortices of opposite sign leads to a loss of strength in the modulation, and eventually to a recovery in the vertical (x-y plane) symmetry of the wake. In mode 2, however, the modulation in the strength of the Karman vortices in each layer is in phase, and thus the initial evolution and the final stage always exhibits a vertical symmetry at each x-y plane.

Three perspective views of the experimentally visualized and numerically calculated position of the interface corresponding to the case of the horizontal (plane of the wake) perturbation (mode 2) are presented in Fig. 7. Notice that the numerical simulation, at least in the early stages of the evolution of the flow, faithfully models the interface, indicating that the inviscid induction of the vorticity appears to be the dominant feature in the early evolution of the wake. The counter-rotating pairs of streamwise vortices are visible in both the near-end view, Fig. 7(b), as well as in the plan view, Fig. 7(c). The undulation in the spanwise vortices

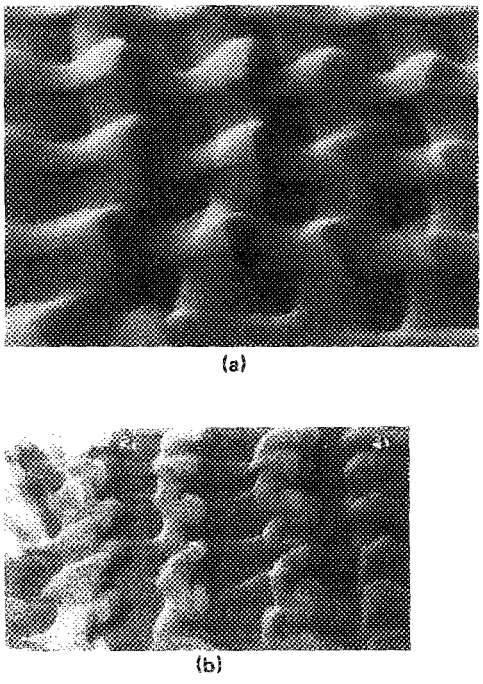

FIG. 6. Perspective view of the experimentally visualized interfaces. (a) Mode 1 (sinusoidal, cross-stream perturbation). (b) Mode 2 (sinusoidal, perturbation in the plane of the wake). Observe that in addition to the existence of streamwise vortex pairs, the spanwise, Karman-like vortices have acquired an undulation along the span.

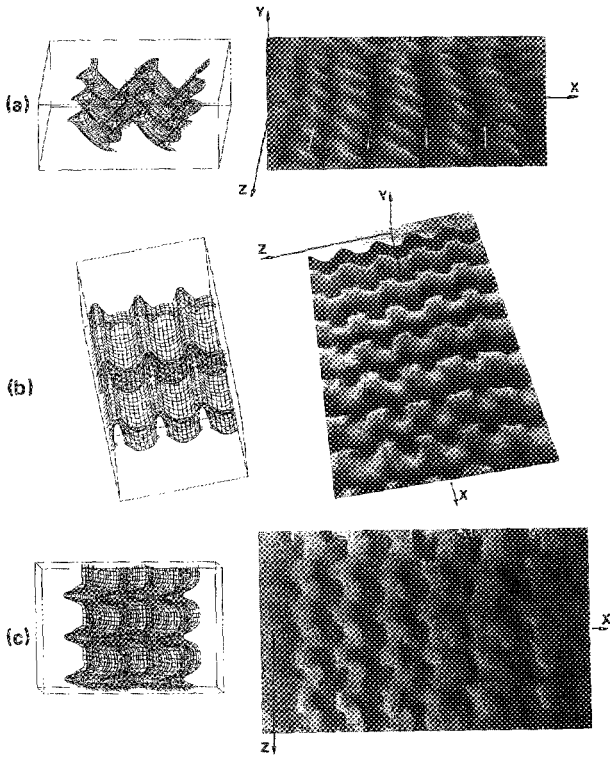

FIG. 7. Mode 2 (sinusoidal perturbation in the plane of the wake). Comparison between the interface visualization and the interface computed with the three-dimensional inviscid vortex filaments dynamics. (a) Perspective side view. (b) Near-end perspective view. (c) Plan view perspective.

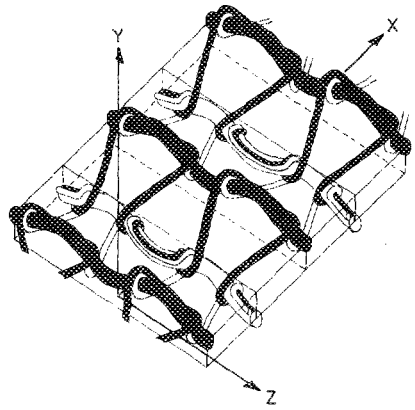

FIG. 8. A schematic perspective view of the vorticity configuration of mode 1 (sinusoidal vertical perturbation). The plane of the wake is the x-z plane and the flow is in the x direction. The vortex filaments of the upper layer appear darker in the figure. Observe the *in-phase* undulation produced in the Karman-like vortices as the streamwise vortex tubes wrap around them.

caused by the evolving streamwise vortex pairs can be observed in the lateral, perspective view, Fig. 7(a), as well as in the near-end, Fig. 7(b). The corresponding comparisons between the interface visualizations and the computed interfaces corresponding to mode 1 were presented elsewhere.[9]

Figures 8 and 9 show a three-dimensional perspective view of the two modes of vorticity resulting from the vertical and horizontal perturbation, respectively. These schematic representations correspond to a late time step comparable to the one of Figs. 1 and 2. Observe in mode 1 that when the streamwise vortices generated through stretching in each layer wrap around two consecutive Karman vortices, the cancellation of vorticity of opposite sign leads to a recovery in the vertical symmetry of the wake. Also notice that in both modes 1 and 2, at this late stage, the strength of the Karman vortices becomes uniform along the span.

For the purpose of clarity, a schematic configuration of the topology of the vorticity field evolving from each mode, in which only one vortex filament of each layer is plotted per

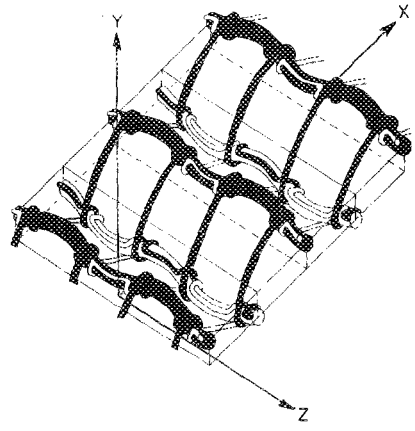

FIG. 9. A schematic perspective view of the vorticity configuration of mode 2 (sinusoidal horizontal perturbation). Observe the *out-of-phase* undulation produced in the Karman-like vortices as the streamwise vortex tubes wrap around them.

braid, is given in Figs. 10(a) and 10(b). Mode 1 is composed of an array of staggered, closed vortex loops of opposite sign located between two consecutive braids. A detail of the closed vortex loops forming on two consecutive braids is seen in the front views of Figs. 10(c) and 10(d). Notice that the circulation Γ alternates signs between consecutive vortices. Mode 2 also shows the existence of closed vortex loops, however, now they are all aligned in the streamwise x direction.

IV. THREE-DIMENSIONAL SUBHARMONIC PERTURBATIONS IN THE PLANE WAKE

In order to investigate to what extent subharmonic perturbations are amplified in the plane wake, and in turn are contributing to the three-dimensional development of the flow, several case studies were analyzed. The first one consisted of a spanwise perturbation of either vertical or horizontal orientation combined with the fundamental and its subharmonic wave in the streamwise direction. In the second case, the wake was subjected to a single wave streamwise forcing plus an oblique wave (or waves) containing the subharmonic of the streamwise mode. The third set of perturbations consisted of a spanwise traveling or standing wave, either with vertical or horizontal orientation, combined with the fundamental and its subharmonic wave in the streamwise direction. In all these cases, the overall induction of the vorticity was found to lead to distinct topologies of the three-dimensional vorticity field of the wake. In the following, the characteristics associated with this three-dimensional evolution of the subharmonic forcing are discussed. For this purpose we have selected to analyze here only the second case study.

The numerical simulation was conducted with a control volume that now contains four wavelengths in the streamwise and one in the spanwise direction. The two sides of the wake centered at $y = +/-0.65$ are again represented as two layers of filaments of unit diameter with an initial separation of 0.25 in the streamwise direction. The main difference, as compared to the previous simulation (Figs. 1 and 2), lies in the form of the initial disturbance. It is now composed of one wave in the streamwise direction with a wavenumber of $2\pi/\lambda = 1.4$ and a pair of subharmonic oblique waves with $2\lambda_x = 2\lambda$ and $\lambda_z = 9.5$ [Figs. 11(a) and 11(b)]. All waves initially have an amplitude of 0.1, and they have the form of a vertical displacement of the filaments in the transverse y direction. The perturbation is identical for both sides of the wake. The phase of the subharmonic is such that its maxima and minima are located, where, caused by the principal wave, the upper layer will form spanwise vortices; consequently its zeros coincide with the locations where

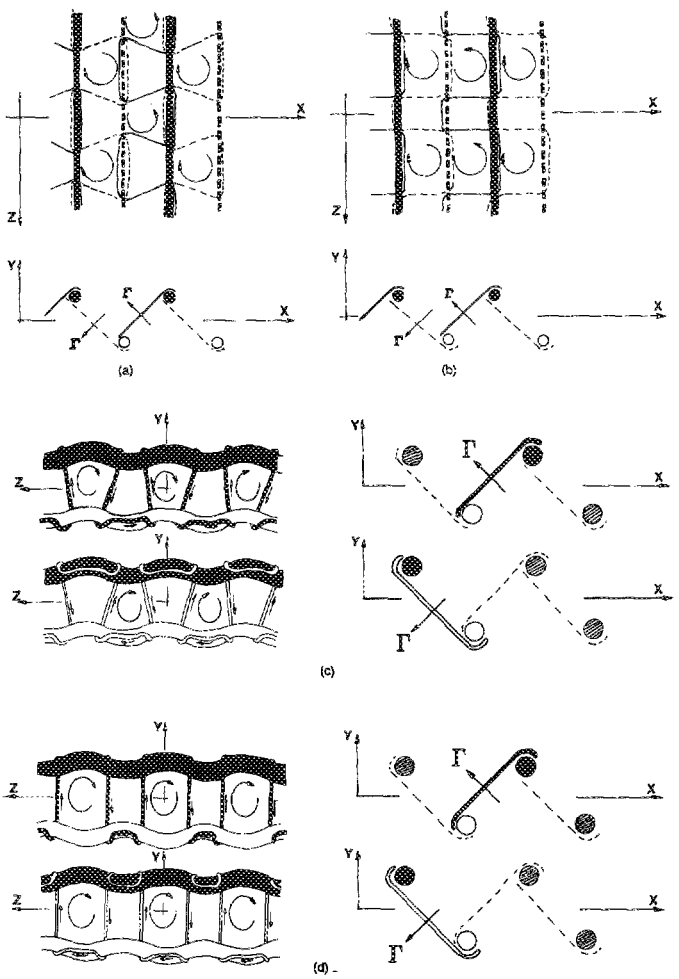

FIG. 10. (a) A schematic plan view of mode 1 showing the staggered array of counter-rotating vortex loops. (b) A schematic view of mode 2 showing an aligned array of counter-rotating vortex loops. (c) Front and end views of mode 1 showing the sign of the circulation of the vortex loops formed in two consecutive braids. (d) Front and end views of mode 2 showing the sign of the circulation of the vortex loops formed in two consecutive braids.

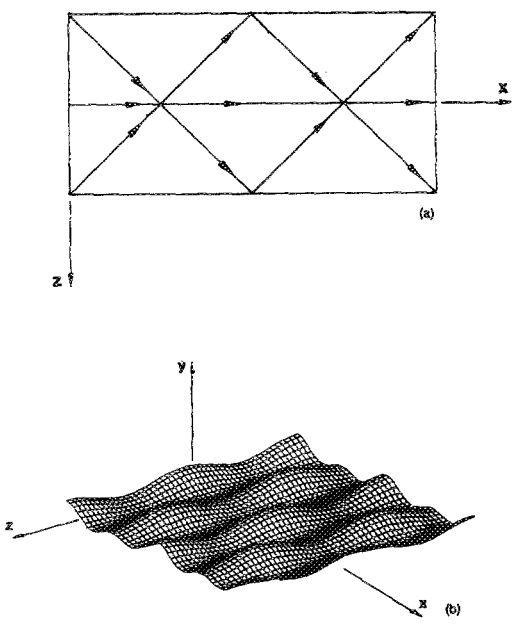

FIG. 11. (a) Initial perturbation leading to a three-dimensional, subharmonic evolution of the flow. The perturbation is composed of one wave in the streamwise direction (λ_x) and a pair of oblique waves containing the subharmonic streamwise mode ($2\lambda_x$). (b) Perspective view of the initial shape of both vorticity layers. To facilitate the visual display of the effect of the combination of the different waves, the transverse scale (y) has been magnified.

the lower layer will evolve into rollers. As a result, the subharmonic waves alternately strengthen and weaken the vortices of the lower layer, whereas the centers of the vortices of the upper layer are alternately being displaced upward and downward (Fig. 12).

The influence of the specific form of the initial perturbation on the nonlinear evolution of the flow manifests itself very soon. Some filaments in the lower layer undergo considerable stretching by periodically approaching the upstream and the downstream roller, thereby causing the alternate strengthening and weakening (see top, side, and front views for $t = 69$, Fig. 12). In the upper layer, on the other hand, the individual filaments experience less stretching, but the centers of the rollers show a wavy dislocation in the transverse y direction. Note the phase shift in this dislocation produced by the subharmonic oblique wave as one moves along the span [Fig. 11(b)]. In the course of the simulation, parts of the most stretched filaments of the lower layer become strongly influenced by the opposite layer, and the interaction of the sides of the wake increases. The filaments in the braid regions of the lower layer now partly cross the center of the wake and begin to wrap around the Karman-like vortices of the upper layer. Again one can recognize a strong interaction of both signs of vorticity in the late stages of the numerical simulation (see Fig. 13 at $t = 84$). Just as for the previously considered case of a single wave perturbation in the spanwise direction, the downstream half of the braid region in the lower layer develops a *lambda*-shaped component of the vorticity, which, as time proceeds, becomes inclined to the plane of the wake. The fact that the upward and downward dislocation of the spanwise rollers continues to grow until the end of our simulation, indicates

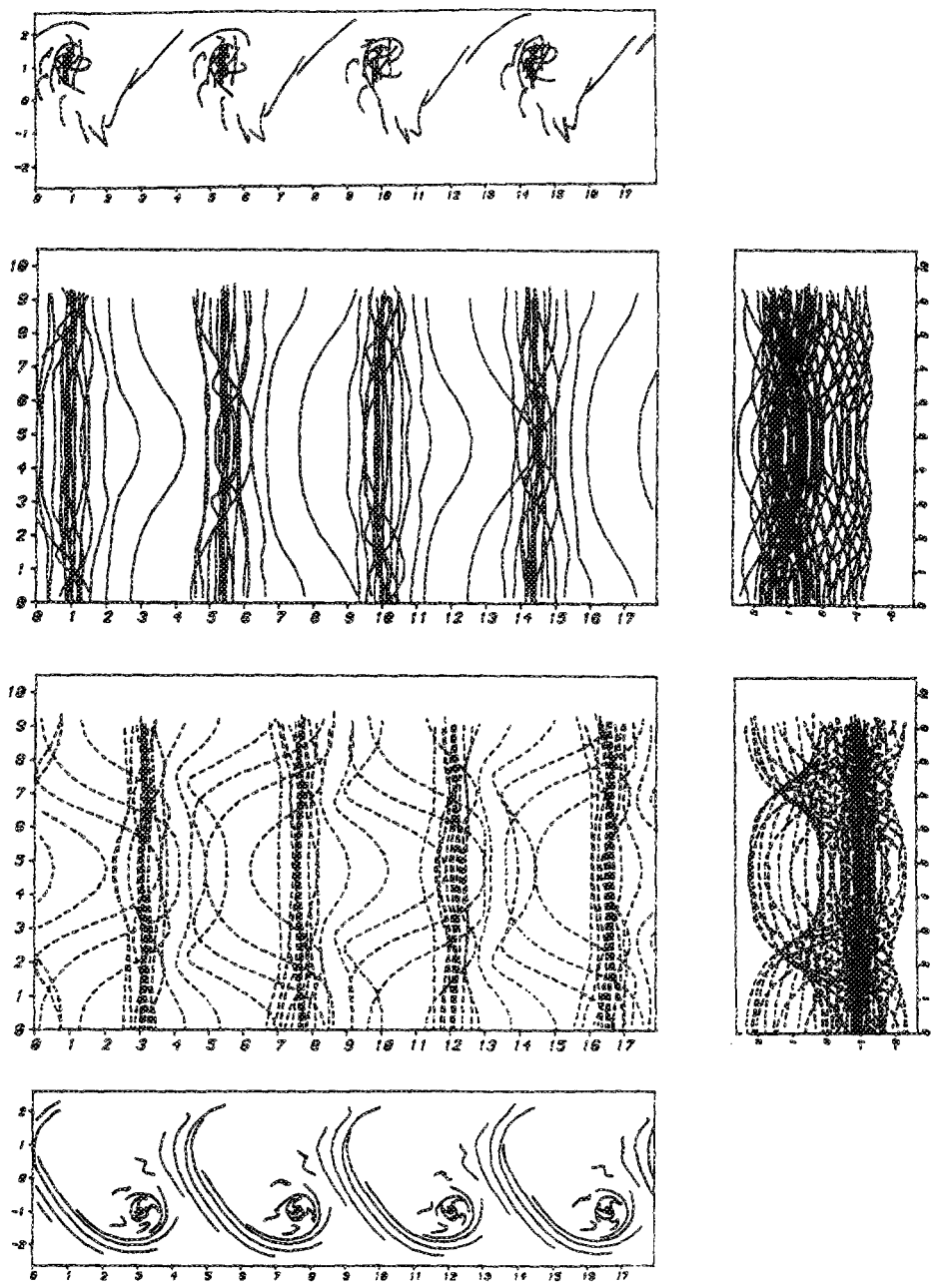

FIG. 12. The subharmonic case. Top, side, and end views of the filaments of the upper and lower layers at time $t = 69$.

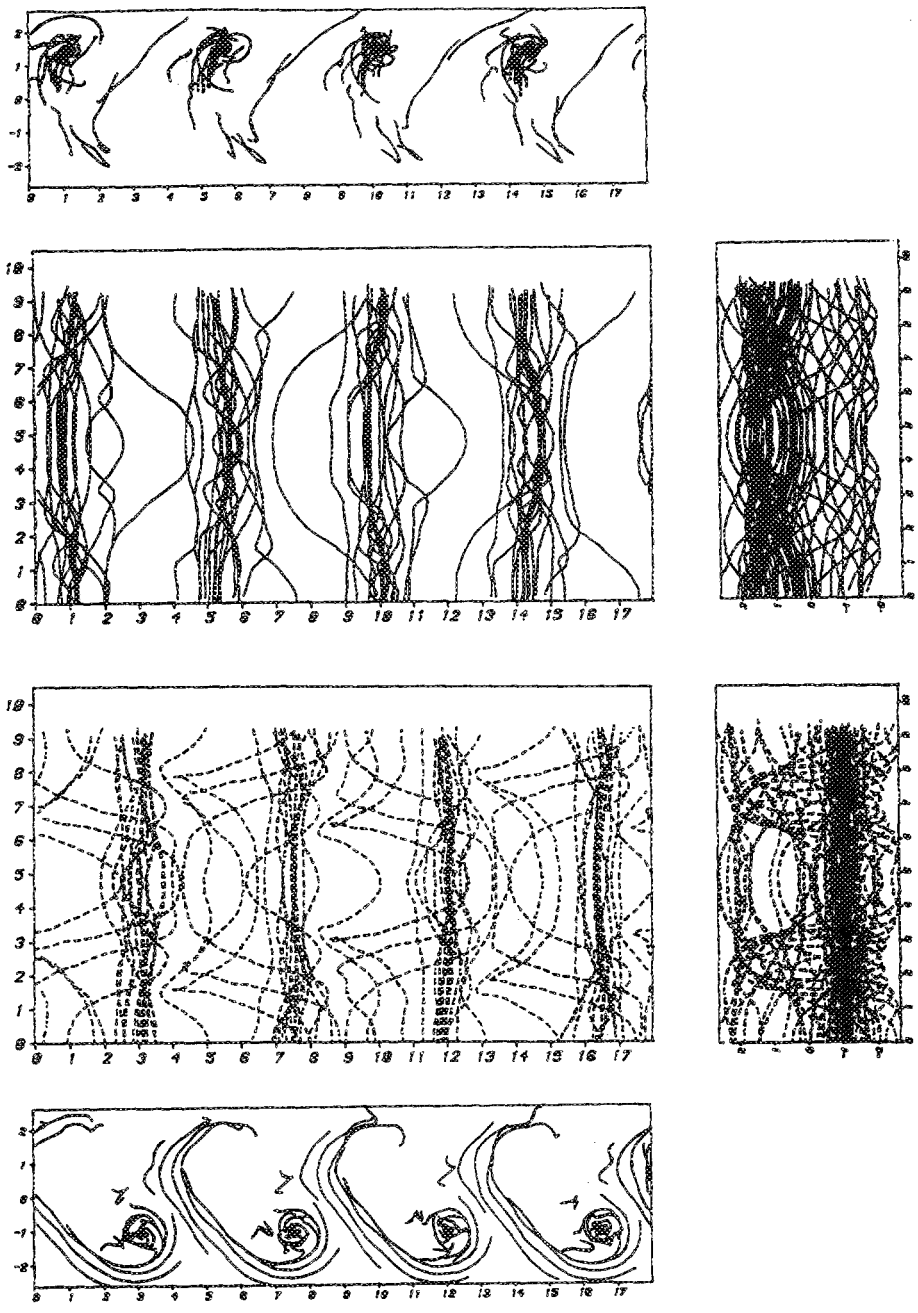

FIG. 13. The subharmonic case, $t = 84$. Note that the filaments of each layer undergo unequal degrees of stretching, whereby most of the streamwise vorticity originates from the lower layer.

that at least the initial stages of a subharmonic mode are amplified in the wake flow. Note also that because of the spanwise phase shift in the vertical dislocation produced by the subharmonic component, the Karman-like vortices of the upper layer exhibit a varicose configuration. Meanwhile, the roles of the lower layer, although experiencing a tearing process, do not undergo a vertical dislocation, thus remaining aligned along the z axis (see end views in Figs. 12 and 13).

In order to be able to compare the numerical simulation and the experimental flow visualizations, we have numerically integrated streak lines. For this purpose, we take the vorticity field at time $t = 59$, extend it periodically in the flow direction, and let it move past an imaginary smoke wire from which particles are released. In this way, we neglect the spatial variation of the vorticity and the corresponding velocity field in the integration procedure. One reason for this approach lies in the limited storage capacity of our computer, which does not allow us to simultaneously access many different time levels of the flow field. However, as clearly demonstrated by Cimbala *et al.*[7] for small growth rates, the spatial variation of streak line patterns is mostly due to the integration effect of the streak lines rather than to the actual spatial variation of the velocity field. Similar to the experimental procedure of Cimbala *et al.*, we assume the smoke wire to be positioned at $y = -1$, which is close to the center of the lower layer of vorticity. At short time intervals, it releases the marker particles, whose trajectories are calculated by a second-order technique, assuming that the smoke particles neither diffuse nor exhibit any inertial effects. Fig-

ure 14(a) shows a top view of the numerically integrated streak line pattern, which should be compared to Cimbala *et al.*,[7] (their Fig. 20). At the beginning, the streak lines closely follow the flow direction. After being convected a short distance, they develop slight kinks while forming areas of increased particle concentration. The staggered patterns formed by these areas indicate the subharmonic character of the flow. Note the close resemblance between this simulation and the configuration detected in parts of Cimbala's[20] smoke visualizations. This indicates that the mechanism responsible for the three-dimensional pattern, observed in the far wake by Cimbala, could be the growth of subharmonic oblique modes. In order to give an impression of the upward and downward motion of the particles, we also present side views of 12 simulated streak lines equally distributed over one spanwise wavelength [Fig. 14(b)]. Again, one can observe the growth of the subharmonic mode contained in the initial perturbation.

V. CONCLUSIONS

We have shown that the wake behind a two-dimensional body subjected to spanwise perturbations may develop three-dimensional vorticity modes of different symmetry properties. These three-dimensional vorticity modes are shown to result from either the effect of single waves or subharmonic streamwise forcing.

For the case of a single wave streamwise forcing, we have shown the existence of two modes of distinct symmetry characteristics. The first mode [Figs. 10(a) and 10(c)] evolves from an antisymmetrical vertical configuration, resulting in the formation of counter-rotating pairs of streamwise vortices that acquire a lambda-shaped structure and are located in the braids connecting consecutive Karman vortices of opposite sign. In addition, an array of closed vortex loops of alternating signs appear in a staggered configuration in the overall topology of the vorticity field. Furthermore, under the effect of the evolving streamwise vortices, the Karman vortices acquire a vertical undulation that is in phase in each side of the wake. The second mode [Figs. 10(b) and 10(d)] evolves from a symmetric vertical configuration, also leading to the formation of counter-rotating pairs of streamwise vortices in the braids connecting consecutive Karman vortices. These streamwise vortex pairs remain parallel to each other while their relative distance is not uniform along the span. In addition, an array of closed vortex loops of alternating signs appears in an aligned configuration, and the Karman vortices acquire a vertical undulation 180° phase shifted between consecutive vortices of opposite sign.

When the wake is subjected to subharmonic streamwise forcing, additional modes of the topology of the vorticity field are shown to exist. The evolution of these modes is characterized by the amplification of the subharmonic component in the presence of the spanwise forcing. These modes exhibit a marked lost of the wake symmetry, whereby the streamwise vortices are preferentially formed from only one of the two vorticity layers composing the wake.

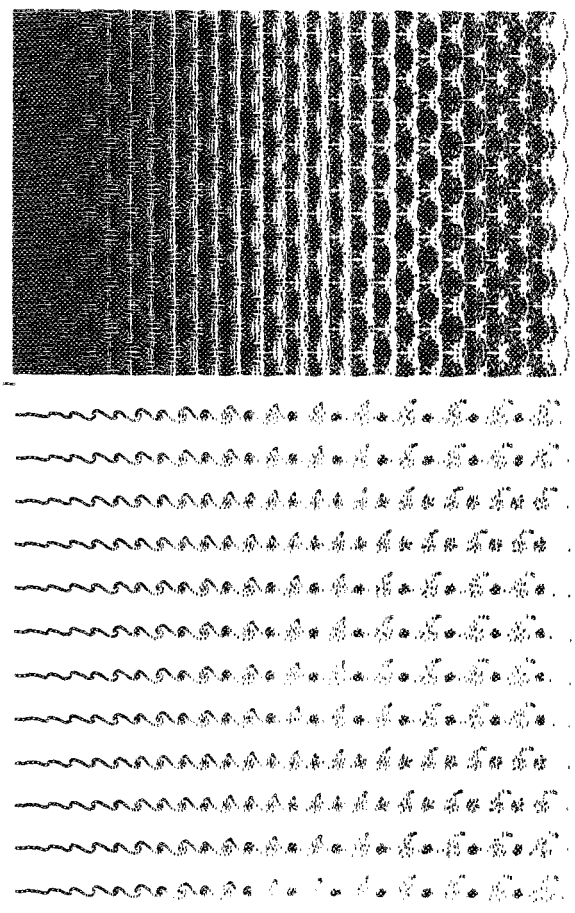

FIG. 14. (a) A top view of the streak lines integrated numerically. The momentumless passive markers have been released at time $t = 59$ at a cross-stream location $y = -1$. Mostly the effect of the lower layer is therefore reflected in the evolution of the markers. (b) Side view of the markers of (a) (only 12 streak lines equally spaced along the span are shown in the figure).

ACKNOWLEDGMENTS

The support for this work was partially from the United Technologies Corporation (to JCL), a grant from the US–Spain Joint Committee for Scientific Cooperation, Grant No. CCA-8510-057 (to JCL), and from NSF Grant No. MSM-8809438 (to EM), and DARPA–URI No. N00014-86-K0754 to Brown University (EM). Computing time was provided by the San Diego Supercomputer Center.

[1] A. Roshko, NACA Report 1191, 1954.
[2] S. Taneda, Prog. Aerosp. Sci. **17**, 287 (1977).
[3] M. L. Grant, J. Fluid Mech. **4**, 149 (1958).
[4] F. Payne and J. Lumley, Phys. Fluids Suppl. **10**, S194 (1967).
[5] A. A. Townsend, J. Fluid Mech. **95**, 515 (1979).
[6] J. C. Mumford, J. Fluid Mech. **137**, 447 (1983).
[7] J. M. Cimbala, H. Nagib, and A. Roshko, J. Fluid Mech. **198**, 265 (1988).
[8] E. Meiburg and J. C. Lasheras, Phys. Fluids **30**, 623 (1987).
[9] E. Meiburg and J. C. Lasheras, J. Fluid Mech. **190**, 1 (1988).
[10] E. Detemple, ISSN Report 0374-1257, No. 84, Max-Planck-Institut für Strömungsforschung, Göttingen, West Germany, 1987.
[11] C. H. K. Williamson, Phys. Fluids **31**, 3165 (1988).

[12] C. H. K. Williamson, J. Fluid Mech. **206**, 579 (1989).
[13] J. A. Ferre and F. Giralt, J. Fluid Mech. **198**, 27 (1989).
[14] B. Marasli, F. H. Champagne, and I. J. Wygnanski, J. Fluid Mech. **198**, 255 (1989).
[15] E. Meiburg, Ph.D. dissertation, Universität Karlsruhe (TH), 1986. Also Report No. DFVLR-FB 86-10, 1986.
[16] E. Meiburg, J. Fluid Mech. **177**, 83 (1987).
[17] J. C. Lasheras, J. S. Cho, and T. Maxworthy, J. Fluid Mech. **172**, 231 (1986).
[18] J. C. Lasheras and H. Choi, J. Fluid Mech. **189**, 53 (1988).
[19] W. T. Ashurst and E. Meiburg, J. Fluid Mech. **189**, 87 (1988).
[20] R. Cimbala, Ph.D. dissertation, California Institute of Technology, Pasadena, 1985.